


Effect of rotational speed on various performance measures in friction stir lap weld of aluminium alloy 6061 using numerical simulation approach

A. Yadav , A. Jain, R. Verma

National Institute of Technology Kurukshetra, Kurukshetra, India

 amit.insan77@gmail.com

ABSTRACT

The quality of a friction stir weld is significantly influenced by the choice of appropriate weld parameters, with rotational speed being one of the key factors. This study aims to examine these elements' influence on physical characteristics of velocity, viscosity, and torque. The performance measures being evaluated include the assessment of maximum weld interface velocity, minimum weld interface viscosity and tool-workpiece interface torque. This study utilises a computational fluid dynamics model to examine the influence of various rotational speeds on the aforementioned performance indicators. The workpiece selected for this study is an Aluminium Alloy 6061, while the tool employed is a truncated conical pin tool featuring a conical shoulder in a lap joint configuration. The study reveals that with an increase in rotational speed from 500 to 2900 RPM, maximum weld interface velocity exhibits an increase with decreasing slope. As the rotational speed increases, the minimum weld interface viscosity decreases with decreasing slope. It is also found that tool-workpiece interface torque decreases with approximately constant slope with increasing rotational speed (500 to 2900 RPM), meaning a linear decreasing trend. The findings of this investigation are validated through a comparative analysis with previously published data. With this information and the resulting conclusions, friction stir welders can deepen their understanding of how rotational speed affects welding quality.

KEYWORDS

friction stir welding • computational fluid dynamics • fluent • finite volume method

Citation: Yadav A, Jain A, Verma R. Effect of rotational speed on various performance measures in friction stir lap weld of aluminium alloy 6061 using numerical simulation approach. *Materials Physics and Mechanics*. 2024;52(6): 114–125.

http://dx.doi.org/10.18149/MPM.5262024_10

Introduction

The friction stir welding (FSW) technique was initially developed in 1991 and subsequently patented by the prestigious organization known as The Welding Institute (TWI) [1]. The purpose of this invention was to achieve robust and durable structures by welding materials with limited welding capabilities, specifically aluminium alloys. This issue is of great importance to various industries, particularly the aerospace sector, as conventional methods are inadequate for welding aluminium alloys or joining incompatible materials like aluminium and magnesium alloys.

During FSW, a rotating tool is gradually inserted into the workpiece until the shoulder comes into contact with the workpiece, as shown in Fig. 1. This position is upheld until the necessary temperature is attained due to the generation of heat through friction and plastic deformation. In order to accomplish the necessary weld, the tool is displaced along the weld line. The term advancing side (AS) is used to describe the side

of a rotating tool that has identical direction as the tangential velocity and traverse speed (TRS). The retreating side (RS) refers to the side of a rotating tool that has a vectorial sense opposite to the tangential velocity and TRS [2]. The workpiece section located ahead of tool is known as leading side, and the section located behind tool is known as trailing side.

Since its inception, a substantial body of research has been dedicated to investigating the impacts of various elements in the FSW process [3–8]. Certain factors are machine-specific, while others, such as spinning velocity and pin geometry, are inherent to the tool [9–15]. Each of these variables influences the transfer of heat and the movement of material, which subsequently has an effect on the microstructure and quality of the weld [16,17]. This study aims to assess the impact of rotational speed (ROS) on various performance measures for aluminium alloy 6061 (AA6061) lap welds using a truncated conical pin with conical shoulder (TCPCS) tool. The variables of interest include maximum weld interface temperature (Max. WIT), maximum weld interface velocity (Max. WIV), minimum weld interface viscosity (Min. WIVis), and tool-workpiece interface torque (TWIT). This study employs the finite volume technique (FVM) of computational fluid dynamics (CFD) as an efficient and time-effective approach [11].

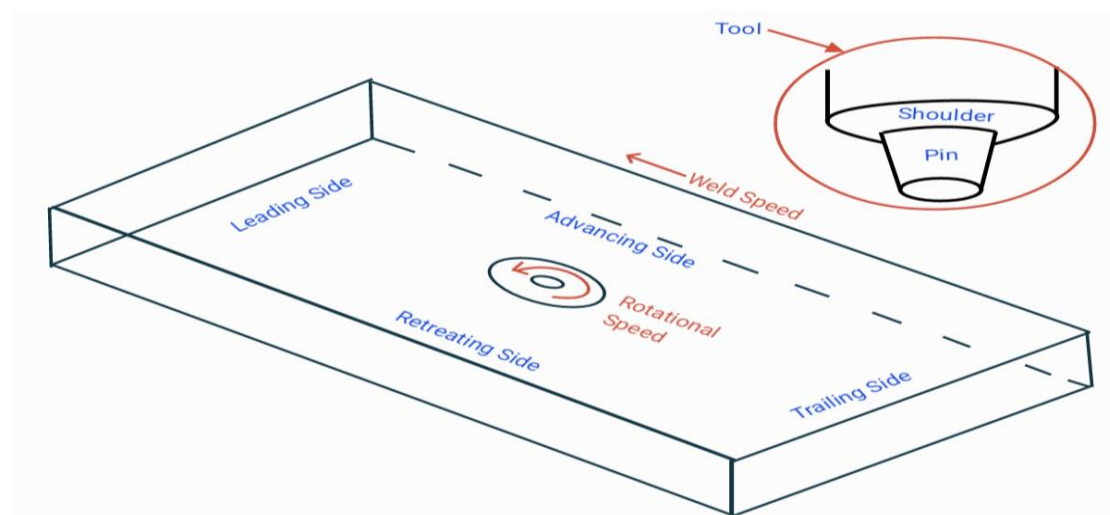


Fig. 1. Schematic representation of the FSW process

Multiple researchers have conducted investigations on FSW. Nandan et al. [12–14] utilised the three dimensional visco-plastic model for butt joints in stainless steel-SS304, AA6061, and mild steel-1018, respectively. The instrument's combined rotational and linear movement revealed a notable imbalance in the temperature distribution surrounding it. In [15], it was conducted a study where they developed a three-dimensional thermo-mechanical model to examine the temperature and material flow in the butt weld of AA6061-T6. Augmenting the ROS while reducing the welding speed results in an intensified stirring motion, hence improving the weld's quality. To avoid defects, the ROS should increase proportionally with the welding speed [15]. J. Zhang et al. [11] developed a computational fluid dynamics model in FLUENT® to analyse the temperature distribution and material flow characteristics of an AA6061-T6 lap joint under the influence of a conical tool. The model does not consider the effect of tool tilt.

The findings suggest that the shoulder surface area is primarily responsible for the majority of heat generation, accounting for 88 % of the total. On the other hand, the regions of the pin's side surface and pin's bottom surface barely account for 10.48 and 1.52 %, respectively. The occurrence of intense material movement is primarily limited to the area near the tool, where material located on tool's front is driven towards RS and then gathers at tool's back [11]. Jain, Pal, and Singh [16] created a model to forecast the forces, spindle torque, temperature, and plastic strain that occur during the butt-welding process of two AA2024-T4 metals. The rise in heat generation rate, as indicated by the temperature distribution, leads to a decrease in forces and spindle torque as the ROS increases. In addition, the conical shape of the pin resulted in a higher material velocity compared to its cylindrical version while requiring less effort during the plunging process Shi and Wu [17] created a transient model to accurately assess the dynamic changes in heat-generation, temperature-distribution, and material-flow during the butt FSW process of AA2024. They also examined how these factors are influenced by process parameters, including TRS and tool ROS. It has been observed that the tool torque rises when the TRS increases, providing that the ROS remains constant. An inverse relationship was seen when the rotating speed increased, assuming that the temperature and pressure remained constant. Hasan [18] conducted a study where he used FSW to simulate the butt joint of AZ31 magnesium alloy. Results showed that the maximum temperature drops as the TRS increases while the ROS remains constant. Roubaiy et al. [19] examined how different welding parameters affect the mechanical properties of a butt joint made by FSW using aluminium 5083-H116. As the ROS increases (assuming the TRS remains constant), the tensile strength and joint efficiency rise while the absorbed energy drops. Conversely, a contrasting effect on TRS was noticed, but the ROS remained unchanged [19]. Nirmal and Jagadesh [20] conducted a study on the percentage elongation, yield strength, and ultimate tensile strength of a dual-phase titanium alloy using FSW on butt joints. The study revealed that when the ROS increases (assuming the TRS remains constant), the yield stress, ultimate tensile stress, and tensile strength also increase, while the percentage elongation drops. An inverse relationship was seen as the TRS increased, assuming the ROS remained constant [20]. Andrade et al. [21] examined the torque and temperature FSW of aluminium alloys belonging to series AA2xxx, AA5xxx, AA7xxx, and AA8xxx. It has been observed that when the ROS increases (assuming the torque sensitivity remains constant), the torque drops but the peak temperature increases. In contrast, there was a reported increase in TRS, assuming that the rotating speed remained constant. Furthermore, it was noted that an increase in workpiece thickness correspondingly leads to an increase in torque. An augmentation in shoulder diameter leads to a corresponding augmentation in peak torque and temperature [21]. H. J. Zhang et al. [22] performed FSW on AA6061 with rotation speeds varying from 1,000 to 6,000 RPM. The study reveals that as the ROS increases (while keeping the TRS constant), the peak temperature also increases. Yadav et al. [23] conducted a study on the tool tilt effect for AA6061 using a tapered cylindrical pin to analyse its impact on heat and material flow. It was discovered that the temperature drops as the tilt angle increases [23].

The literature review indicates that no previous study has examined the impact of different ROS on velocity, viscosity, and torque for AA6061. Specifically, this study focuses

on the use of a TCPCS tool for a lap joint. The current study investigates the impact of different ROSs (ranging from 500 to 2900 RPM) on several performance parameters, including maximum weld interface velocity, minimum weld interface viscosity, and tool-workpiece interface torque. Solidworks® 2017 is utilised for the purpose of geometric modeling, whereas the CFD programme FLUENT® is employed specifically for FVM modeling [24]. The effect of changing ROS is evaluated by analysing these performance indicators. The novelty of this work will be elucidated in the next section:

This study examines the impact of tilt angle and slip in lap weld. The impact of the shoulder's side surface on heat generation is also taken into account. An analysis is conducted on the performance metrics of the lap weld's weld surface. Prior studies have examined the maximum temperature attained within a workpiece. The range of ROS is dictated by the recrystallization and solidus temperatures of the workpiece formed at the weld surface. This comprehensive study examines the impact of all significant input elements on the geometry of FSWs and the tool used, as well as their influence on many performance metrics.

Numerical modeling

As a result of the intricate nature of the practical arrangement, a cost and time-efficient technique of numerical modelling is utilised [13,25]. This particular portion provides a numerical model for friction stir lap weld of AA6061 using a TCPCS tool. It includes the necessary assumptions, boundary-conditions, material-parameters and model validation.

Description of model

Utilising numerical modeling allows for the efficient and effortless visualisation of temperature distribution, material movement, as well as stress and strain analysis [11]. It offers valuable understanding into the operation of the process. The impact of different ROS on velocity, viscosity, and torque was analysed using the commercial CFD FLUENT® software. Figure 2 illustrates the simulation model. AA6061 plates are utilised. The dimensions of each plate are $200 \times 100 \times 5 \text{ mm}^3$. When joined in a lap arrangement, the measurements are $200 \times 100 \times 10 \text{ mm}^3$ [11]. The parameters for the FSW technique are provided in Table 1. The selection of these characteristics is based on a thorough evaluation of the pertinent literature [17,18].

Table 1. Process parameters employed

| Process parameter | Value |
|------------------------------|-------|
| Diameter of shoulder, mm | 25 |
| Conical angle of shoulder, ° | 2 |
| Tilt angle, ° | 0.25 |
| Pin length, mm | 5 |
| Root diameter of pin, mm | 8 |
| Tip diameter of pin, mm | 6 |
| Traverse speed, m/s | 0.05 |
| Plunge depth, mm | 0.375 |

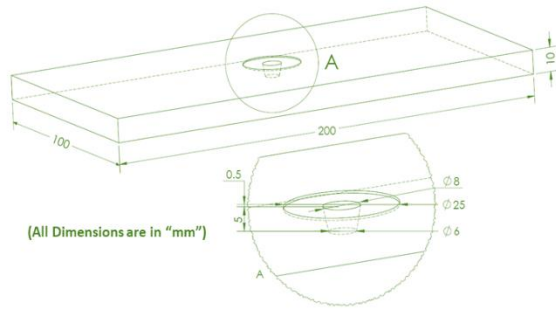


Fig. 2. Model's schematic sketch

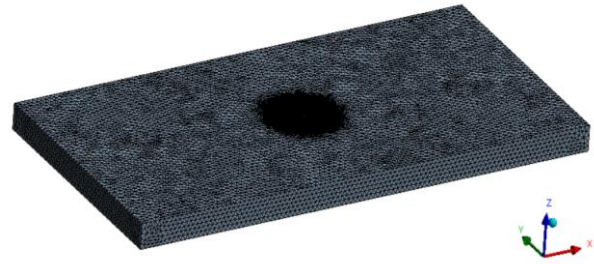


Fig. 3. Mesh used

The Realisable k-epsilon viscous model is employed to simulate the flow of material in a transient state. Mesh with tetrahedron-cells is utilised, with fine mesh at the interface between the tool and the workpiece, as depicted in Fig. 3. The present work adheres to the following assumptions.

The process is a quasi-steady process, meaning that the rate of heat generation remains constant. Plasticized material is classified as non-Newtonian, incompressible, and visco-plastic. The material is presumed to exhibit the characteristics of a non-Newtonian fluid, where its viscosity is influenced by both temperature and strain rate. There is a condition of partial slip between the tool and the workpiece. The upper, bottom, and side surfaces of the workpiece have a free slip condition. The outlet boundary assumes a value of zero pressure.

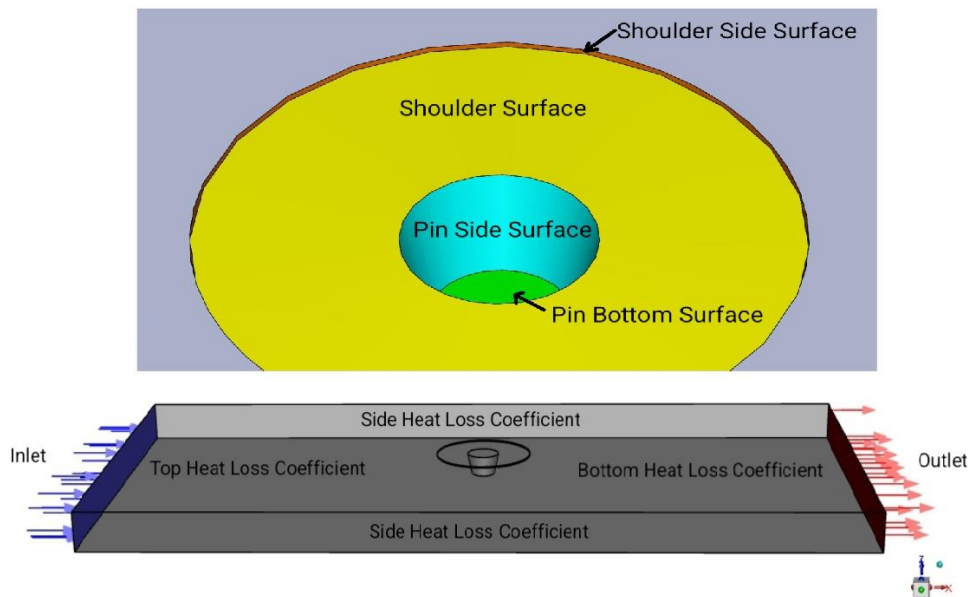


Fig. 4. Model's parts and boundary conditions

Boundary conditions and material properties. In order to make precise predictions about welding, it is crucial to employ realistic boundary conditions [18]. Figure 4 displays the parts and boundaries imposed on the model.

The inlet boundary condition of flow is defined as follows:

$$u = u_{weld}, v = 0, w = 0, \tag{1}$$

where welding velocity is represented by u_{weld} , whereas the velocity intensities in the X, Y, and Z directions are represented by u , v , and w , respectively.

The tool periphery velocity, which is the combined effect of the tool's angular velocity and the welding speed, is provided below:

$$u_i = \omega r \sin\theta - u_{weld}, v_i = \omega r \cos\theta, w_i = 0. \quad (2)$$

The value of r is such that $r_1 < r < r_3$. The variables u_i , v_i and w_i denote vectors of velocity in the X, Y, and Z directions. The index notation "i" means a specific location on tool's surface where the tool's combined ROS and the TRS are determined. r_1 represents the radius of tool shoulder; r_3 represents the radius of pin bottom; θ is the angle between the horizontal direction vector from the tool axis to any point on the cylindrical surface. In the weld direction, θ is equal to zero.

Tool periphery velocity when tool tilt angle (ξ) and contact state variable (δ) are considered are represented [13]:

$$u_i = (1 - \delta)((\omega r \sin\theta) \cos \xi - u_{weld}), \quad (3)$$

$$v_i = (1 - \delta)\omega r \cos\theta, \quad (4)$$

$$w_i = (1 - \delta)(\omega r \sin\theta) \sin \xi, \quad (5)$$

$$\delta = 0.9(0.31e^{\omega r/1.87} - 0.026). \quad (6)$$

The viscosity (η) is determined using below equations [26–28]:

$$\eta = \frac{\sigma}{3\bar{\epsilon}}, \quad (7)$$

$$\sigma \text{ (flow stress)} = \frac{1}{\beta} \ln \left\{ \left(\frac{Z}{A} \right)^{\frac{1}{n}} + \left(1 + \left(\frac{Z}{A} \right)^{\frac{2}{n}} \right)^{\frac{1}{2}} \right\}, \quad (8)$$

$$Z \text{ (Zener Hollomon parameter)} = \bar{\epsilon} e^{\left(\frac{Q}{RT} \right)}, \quad (9)$$

$$\bar{\epsilon} \text{ (strain rate)} = \left(\frac{2}{3} \epsilon_{ij} \epsilon_{ij} \right)^{\frac{1}{2}}, \quad (10)$$

where T represents temperature (K), A , β , and n are constants that describe the material properties, Q is an activation energy that does not depend on temperature, R is the gas constant. These equations are implemented through the use of user defined functions (UDF). Table 2 provides the material-constants and properties of AA6061 [29].

Table 2. Material-constants and properties for aluminium alloy 6061

| Parameter | Value |
|---|--------------------|
| Material-constants: | |
| A, s^{-1} | 2.41×10^8 |
| n | 3.55 |
| $Q, J \cdot mol^{-1}$ | 1.45×10^5 |
| B, MPa | 0.045 |
| Material density $\rho, kg \cdot m^{-3}$ | 2700 |
| Gas constant $R, J \cdot K^{-1} \cdot mol^{-1}$ | 8.314 |

The heat created during the FSW process is distributed over many regions. The tool's contacting surface with the workpiece is partitioned into three sections: bottom shoulder surface (SS), pin side surface (P_{SS}), and pin bottom surface (P_{BS}) (Fig. 4). The SS is subdivided into two sections: shoulder with conical surface (S_{CS}) and shoulder with flat surface (S_{FS}). All these sections exhibit partial sticking-sliding contact. The heat produced by different sources is provided below:

$$Q_{total} = \delta Q_{sticking} - (1 - \delta) Q_{sliding}. \quad (11)$$

The symbol δ represents the contact state variable. When the slip coefficient (δ) is equal to zero, heat is only generated through friction. When the value of δ is equal to 1 (indicating a stick), all heat is produced only through the deformation of the plastic material [30].

The assumed maximum yielding shear stress is:

$$\tau_b = \frac{\sigma_s}{\sqrt{3}} \quad (12)$$

where σ_s represents the material's yield stress at its melting point temperature [31].

The δ at S_{CS} has been assigned a value of 0.35 [11]. The heat-flux (W/m^2) at this section is:

$$q_{S_{CS}} = \frac{[\delta_{CSS}\tau_b + (1-\delta_{CSS})\mu P]2\omega[(r_1^3 - r_2^3)(1 + \tan\alpha')]}{3(r_1^2 - r_2^2)} \quad (13)$$

At P_{SS} , δ is equal to 0.5 [11]. The heat-flux (W/m^2) at this section is:

$$q_{P_{SS}} = \frac{2\delta_{PSS}\omega\tau_b(r_2^3 - r_3^3)\cos\alpha}{3(r_2^2 - r_3^2)} + \frac{2(1-\delta_{PSS})\mu P\omega(r_2^3 - r_3^3)}{3(r_2^2 - r_3^2)} \quad (14)$$

At P_{BS} , δ has a value of 0.35 [11]. The heat-flux (W/m^2) at this section is:

$$q_{P_{BS}} = \frac{2\omega r_3(\delta_{PBS}\tau_b + (1-\delta_{PBS})\mu P)}{3} \quad (15)$$

where μ (0.4) is coefficient of friction [11], P is plunge pressure (Pa), ω is ROS (rad/s) and α' is cone angle of shoulder ($\alpha' = 0$ for S_{FS}). A plunging pressure of 12 MPa is taken here [11].

The specific-heat (C_p) equation for AA6061 is shown below [13]:

$$C_p = 929 - 0.627T + 1.481 \times 10^{-3}T^2 - 4.33 \times 10^{-8}T^3 \quad (16)$$

The thermal-conductivity (k) equation for AA6061 is shown below [13]:

$$k = 25.22 + 0.3978T + 7.358 \times 10^{-6}T^2 - 2.518 \times 10^{-7}T^3 \quad (17)$$

The boundary condition for heat exchange between the top surface of the workpiece and the environment is convective as well as radiative heat transfer [13]. The heat exchange between the bottom and side surfaces of the workpiece is conductive (due to contacts of jigs and fixtures) and convective heat transfer, respectively. All these heat exchanges are converted to convective form as shown below [13]:

$$k \frac{\partial T}{\partial z} = h_t(T - T_0), \quad (18)$$

$$k \frac{\partial T}{\partial z} = h_b(T - T_0), \quad (19)$$

$$k \frac{\partial T}{\partial z} = h_s(T - T_0). \quad (20)$$

where h_t , h_b and h_s are coefficients of heat dissipation at workpiece's top, bottom and side surface, respectively. T_0 is the environmental temperature (300 K).

In this study, $h_b = 150 W/m^2K$, and $h_t = h_s = 80W/m^2K$. The external emissivity of workpiece top surface is 0.09 [32].

Model validation

Validation of current model is done with the work by J. Zhang et al. [11]. They created a 3D CFD model in FLUENT® to understand the temperature-field and material-flow behaviour of an AA6061-T6 lap joint subjected to a conical tool (neglecting tool tilt effect). In the present study, the above work is replicated, and upon validating the current methodology and procedure, additional fixed input parameters (tilt angle and plunge depth) are introduced. The temperature distribution and material flow velocity data

closely correspond to those reported data. Figure 5 compares the present and validated studies' temperature distributions. Thus, numerical-modeling methods are satisfactory.

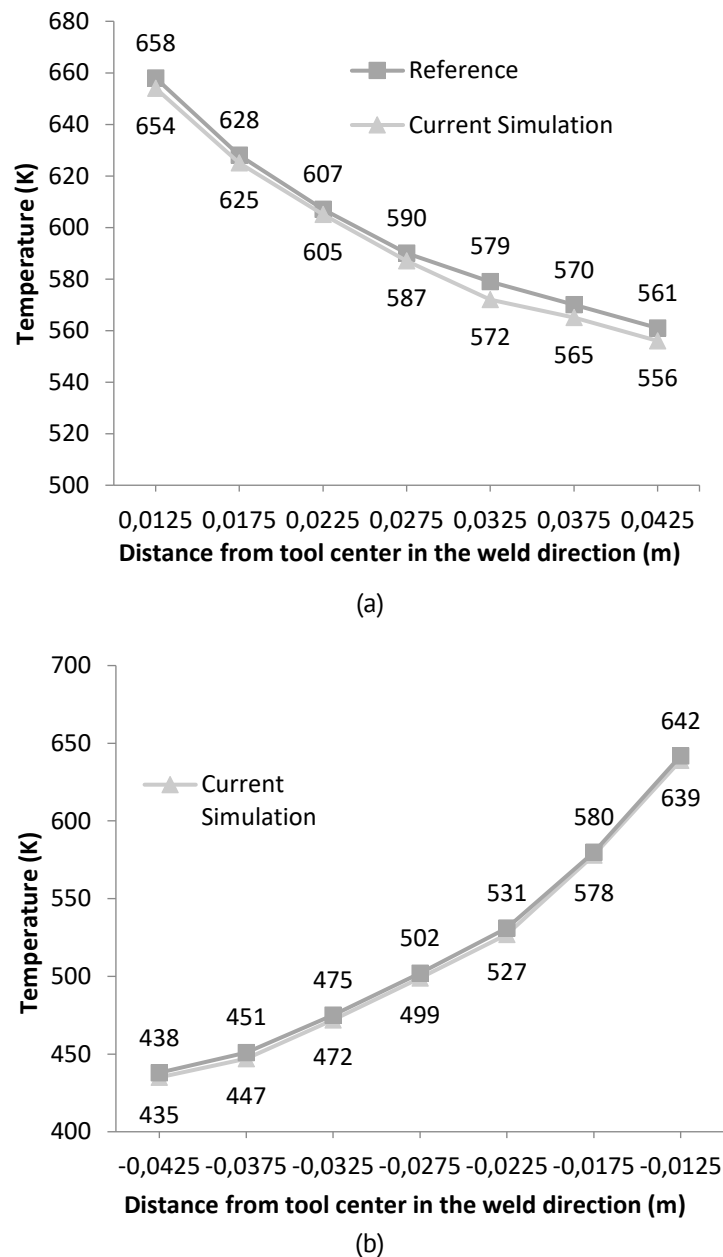


Fig. 5. Comparison of weld temperature for present study and reference study [11]: (a) temperature at workpiece's top surface on trailing side, (b) temperature at workpiece's top surface on leading side

Results and Discussion

This part of the article presents ROS's influence on maximum velocity, minimum viscosity and torque as performance measures. The range of ROS is selected from 500 to 2900 RPM range as below 500 RPM ROS, temperature at weld surface (surface joining two weld plates in lap joint) reaches below its recrystallization temperature (0.5 melting point temperature) for alloys, i.e., 462.5 K and above 2900 RPM ROS, temperature of workpiece increases above its solidus temperature (855 K for AA6061).

Effect of rotational speed

To study the effect of ROS on maximum weld interface velocity, minimum weld interface viscosity and tool-workpiece interface torque, all other input parameters such as TRS, tilt angle and plunge depth are kept at their average value of 0.05 m/s, 0.25° and 0.375 mm, respectively. Table 3 summarizes considered performance measures as varying ROS is varied from 500 to 2900 RPM.

Table 3. Effect of rotational speed on maximum weld interface velocity, minimum weld interface viscosity and tool-workpiece interface torque as performance measures

| Rotational speed, RPM | Max. weld interface velocity, m/s | Min. weld interface viscosity, Kg/(ms) | Tool-workpiece interface torque, Nm |
|-----------------------|-----------------------------------|--|-------------------------------------|
| 500 | 0.1438 | 696164 | 45.6 |
| 900 | 0.2234 | 174093 | 40.22 |
| 1300 | 0.2962 | 75616 | 35.41 |
| 1700 | 0.3615 | 46734 | 32.06 |
| 2100 | 0.4185 | 36169 | 29.68 |
| 2500 | 0.4662 | 29048 | 27.04 |
| 2900 | 0.5038 | 23901 | 26.04 |

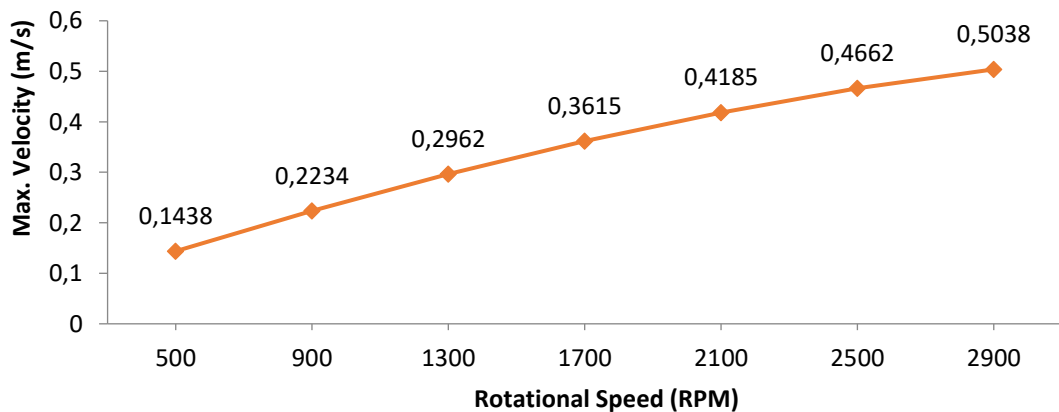


Fig. 6. Effect of tool rotational speed on maximum weld interface velocity (material flow) during FSW

Figure 6 shows the effect of ROS on maximum weld interface velocity. The value of maximum weld interface velocity increases but with a decreasing slope on increasing ROS from 500 to 2900 RPM. The reason for this behaviour is explained as follows. From Eqs. (3)–(5), it is known that resultant velocity is dependent on tool peripheral velocity in the axial directions (x, y and z). This resultant velocity governs maximum velocity performance measure. From Eqs. (3)–(5), it is found that peripheral tool velocity in axial directions is dependent on ROS (ω) and contact state variable (δ), provided all other parameters (traverse speed, tilt angle, etc.) remains constant. The value of contact state variable varies between 0 and 1. This contact state variable is further dependent on ROS, as shown by Eq. (6). Tool peripheral velocity in the axial direction is directly proportional to ROS, and contact state variable is exponentially directly dependent on ROS (meaning

contact state variable is inversely dependent on maximum velocity performance measure, Eq. (6).

The effect of ROS on minimum weld interface viscosity is shown in Fig. 7. It indicates that as ROS increases, minimum weld interface viscosity decreases with decreasing slope. This is due to the fact that at low ROS and at constant traverse speed, tilt angle and plunge depth, the heat flux generation is minimum. This results in a low strain rate and lower temperature, which in turn results in higher viscosity at a low ROS (Eqs. (7)–(10)). As the ROS increases, the temperature and strain rate increase, resulting in lower viscosity. The critical viscosity above which no significant plastic flow takes place is typically around $5 \cdot 10^6$ Pa/s for AA6061 [13].

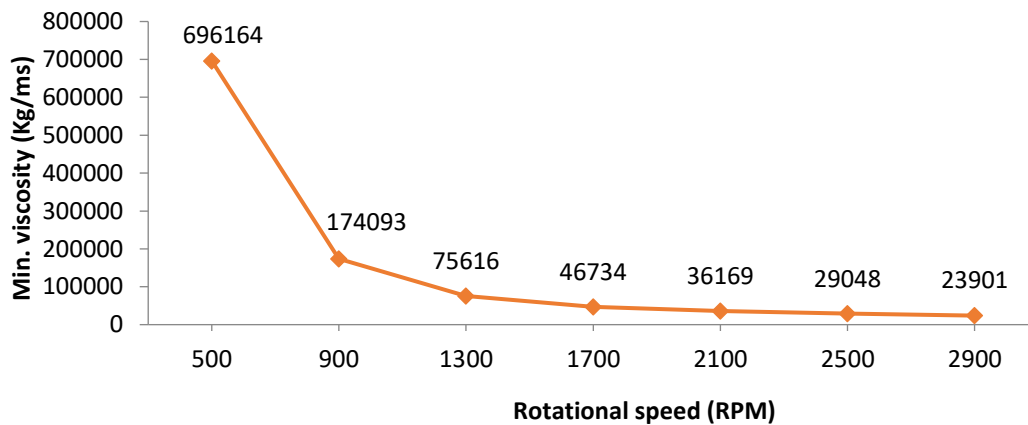


Fig. 7. Effect of tool rotational speed on maximum weld interface velocity

Figure 8 shows the effect of ROS on tool-workpiece interface torque. It indicates that torque decreases with approximately constant slope with increasing the ROS (200 to 2000 RPM), meaning a linear decreasing trend. This is due to the fact that as viscosity decreases with increasing ROS at constant traverse speed, torque at the tool-workpiece interface decreases due to softening of the material.

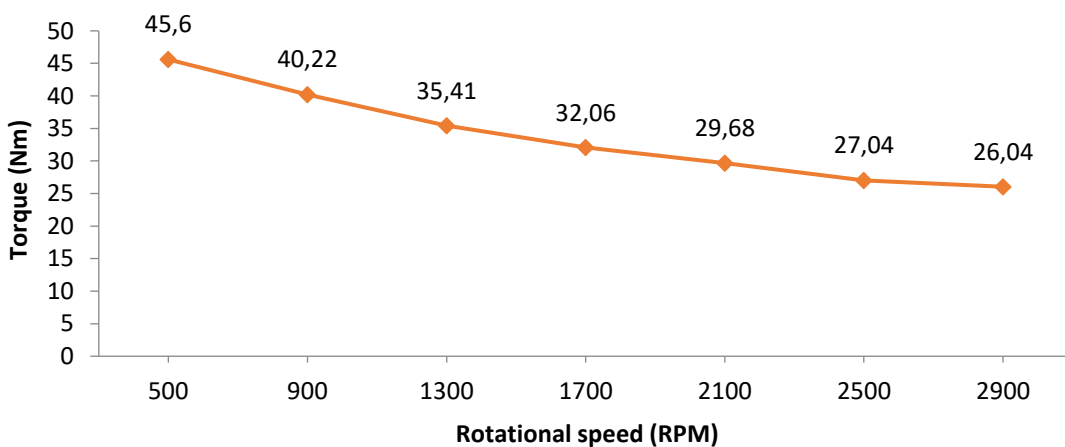


Fig. 8. Effect of tool rotational speed on tool-workpiece interface torque

Conclusions

This investigation studies the effect of varying ROS on maximum weld interface velocity, minimum weld interface viscosity and tool-workpiece interface torque as performance measures. The following conclusions are drawn from the study:

1. with an increase in ROS from 500 to 2900 RPM, maximum weld interface velocity increases but with a decreasing slope;
2. with increase in ROS, minimum weld interface viscosity decreases with decreasing slope. A significant drop in minimum viscosity occurs between 500 and 1300 RPM;
3. tool-workpiece interface torque decreases with the approximately constant slope with increasing ROS (500 to 2900RPM), meaning a linear decreasing trend.

References

1. Schillings Tsang. Friction welding. In: Welding, Brazing, and Soldering. *ACM Internatinal*. 1993. p.315-317.
2. Nandan R, DebRoy T, Bhadeshia HKDH. Recent advances in friction-stir welding - Process, weldment structure and properties. *Prog. Mater. Sci.* 2008;53(6): 980–1023.
3. Zhang XX, Wu LH, Andrä H, Gan WM, Hofmann M, Wang D, Ni DR, Xiao BL, Ma ZY. Effects of welding speed on the multiscale residual stresses in friction stir welded metal matrix composites. *Journal of Materials Science & Tech.* 2019;35: 824–832.
4. Buffa G, Campanile G, Fratini L, Prisco A. Friction stir welding of lap joints: Influence of process parameters on the metallurgical and mechanical properties. *Mater Sci Eng A.* 2009;519: 19–26.
5. Keivani R, Bagheri B, Sharifi F, Ketabchi M, Abbasi M. Effects of pin angle and preheating on temperature distribution during friction stir welding operation. *Trans Nonferrous Met Soc China.* 2013;23(9): 2708–2713.
6. Shi L, Wu CS, Liu HJ. The effect of the welding parameters and tool size on the thermal process and tool torque in reverse dual-rotation friction stir welding. *Int J Mach Tools Manuf.* 2015;91: 1–11.
7. Kadian AK, Puri G, Das S, Biswas P. Effect of tool geometry and process parameters on the material flow of friction stir welding. In: *5th International and 26th All India Manufacturing Technology, Design and Research Conference (AIMTDR 2014)*. Assam, India: IIT Guwahati; 2014. p.12–14.
8. Zhang S, Shi Q, Liu Q, Xie R, Zhang G, Chen G. Effects of tool tilt angle on the in-process heat transfer and mass transfer during friction stir welding. *Int J Heat Mass Transf.* 2018;125: 32–42.
9. Sun Z, Wu CS, Kumar S. Determination of heat generation by correlating the interfacial friction stress with temperature in friction stir welding. *J Manuf Process.* 2018;31: 801–811.
10. Zhai M, Wu CS, Su H. Influence of tool tilt angle on heat transfer and material flow in friction stir welding. *J Manuf Process.* 2020;59: 98–112.
11. Zhang J, Shen Y, Li B, Xu H, Yao X, Kuang B, Gao J. Numerical simulation and experimental investigation on friction stir welding of 6061-T6 aluminum alloy. *Mater Des.* 2014;60: 94–101.
12. Nandan R, Roy GG, Lienert TJ, Debroy T. Numerical modelling of 3D plastic flow and heat transfer during friction stir welding of stainless steel. *Sci. Technol. Weld Join.* 2006;11(5): 526–537.
13. Nandan R, Roy GG, Debroy T. Numerical simulation of three dimensional heat transfer and plastic flow during friction stir welding. *Metall. Mater. Trans. A.* 2006;37(4): 1247–1259.
14. Nandan R, Roy GG, Lienert TJ, Debroy T. Three-dimensional heat and material flow during friction stir welding of mild steel. *Acta Mater.* 2007;55(3): 883–895.
15. Zhang Z, Zhang HW. Numerical studies on controlling of process parameters in friction stir welding. *J. Mater. Proc. Tech.* 2009;209(1): 241–270.
16. Jain R, Pal SK, Singh SB. A study on the variation of forces and temperature in a friction stir welding process : A finite element approach. *J. Manuf. Process.* 2016;23: 278–286.
17. Shi L, Wu CS. Transient model of heat transfer and material flow at different stages of friction stir welding process. *J Manuf Process.* 2017;25: 323–339.
18. Hasan AF. CFD modelling of friction stir welding (FSW) process of AZ31 magnesium alloy using volume of fluid method. *J. Mater. Res. Technol.* 2019;8(2): 1819–1827.
19. Roubaïy AOA, Nabat SM, Dl A. ScienceDirect An Investigation into Friction Stir Welding of Aluminium

- Alloy 5083-H116 Similar Joints. *Mater Today Proc.* 2020;22: 2140–2152.
20. Nirmal K, Jagadesh T. Materials Today : Proceedings Numerical simulations of friction stir welding of dual phase titanium alloy for aerospace applications. *Mater Today Proc.* 2021;46: 4702-4708.
21. Andrade DG, Leitão C, Dialami N, Chiumenti M, Rodrigues DM. Modelling torque and temperature in friction stir welding of aluminium alloys. *Int J Mech Sci.* 2020;182: 105725.
22. Zhang HJ, Sun SL, Liu HJ, Zhu Z, Wang YL. Characteristic and mechanism of nugget performance evolution with rotation speed for high-rotation-speed friction stir welded 6061 aluminum alloy. *J Manuf Process.* 2020;60: 544–552.
23. Yadav A, Jain A, Verma R. Effect of tilt angle for conical pin tool with a conical shoulder on heat transfer and material flow using numerical simulation in friction stir welding. *Materials Physics and Mechanics.* 2023;51(3): 126–145.
24. Kumar A, Bansal SN, Chandraker R. Computational modeling of blast furnace cooling stove based on heat transfer analysis. *Materials Physics and Mechanics.* 2012;15(1): 46–65.
25. Arora A, Nandan R, Reynolds AP, DebRoy T. Torque, power requirement and stir zone geometry in friction stir welding through modeling and experiments. *Scr Mater.* 2009;60(1): 13–16.
26. Thomas WM, Johnson KI, Wiesner CS. Friction stir welding-recent developments in tool and process technologies. *Adv Eng Mater.* 2003;5(7): 485–490.
27. Sheppard T, Wright DS. Determination of flow stress: Part 1 constitutive equation for aluminium alloys at elevated temperatures. *Metals Technology.* 1979;6(1): 215–223.
28. Sheppard T, Jackson A. Constitutive equations for use in prediction of flow stress during extrusion of aluminium alloys. *Materials Science and Technology.* 1997;13(3): 203–209.
29. Tello KE, Gerlich AP, Mendez PF. Constants for hot deformation constitutive models for recent experimental data. *Sci Technol Weld Join.* 2010;15(3): 260–266.
30. Hamilton C, Dymek S, Sommers A. A thermal model of friction stir welding in aluminum alloys. *Int. J. Mach. Tools Manuf.* 2008;48(10): 1120–1130.
31. Neto DM, Neto P. Numerical modeling of friction stir welding process: A literature review. *Int. J. Adv. Manuf. Technol.* 2013;65(1–4): 115–126.
32. Yang CL, Wu CS, Lv XQ. Numerical analysis of mass transfer and material mixing in friction stir welding of aluminum/magnesium alloys. *J Manuf Process.* 2018;32: 380–394.

About Authors

Amit Yadav  **Sc**

Researcher (National Institute of Technology Kurukshetra, Kurukshetra, India)

Ajai Jain **Sc**

PhD, Professor (National Institute of Technology Kurukshetra, Kurukshetra, India)

Rajiv Verma **Sc**

PhD, Professor (National Institute of Technology Kurukshetra, Kurukshetra, India)